Minimally Invasive Method of Determining Blood Input Function from PET Images in Rodents

Joonyoung Kim, PhD; Pilar Herrero, MS; Terry Sharp, RT; Richard Laforest, PhD; Douglas J. Rowland, PhD; Yuan-Chuan Tai, PhD; Jason S. Lewis, PhD; and Michael J. Welch, PhD

Mallinckrodt Institute of Radiology, Washington University School of Medicine, St. Louis, Missouri

For cardiovascular research on rodents, small-animal PET has limitations because of the inherent spatial resolution of the system and because of cardiac motion. A factor analysis (FA) technique for extracting the blood input function and myocardial time–activity curve from dynamic small-animal PET images of the rodent heart has been implemented to overcome these limitations. **Methods:** Six Sprague–Dawley rats and 6 BALB/c mice underwent dynamic imaging with ^{18}F-FDG (n = 6) and 1-^{11}C-acetate (n = 6). From the dynamic images, blood input functions and myocardial time–activity curves were extracted by the FA method. The accuracy of input functions derived by the FA method was compared with that of input functions determined from serial blood samples, and the correlation coefficients were calculated. **Results:** Factor images (right ventricle, left ventricle, and myocardium) were successfully extracted for both ^{18}F-FDG and 1-^{11}C-acetate in rats. The correlation coefficients for the input functions were 0.973 for ^{18}F-FDG and 0.965 for 1-^{11}C-acetate. In mice, the correlation coefficients for the input functions were 0.930 for ^{18}F-FDG and 0.972 for 1-^{11}C-acetate. **Conclusion:** The FA method enables minimally invasive extraction of accurate input functions and myocardial time–activity curves from dynamic microPET images of rodents without the need to draw regions of interest and without the possible complications of surgery and repeated blood sampling.

Key Words: rodent; microPET; blood input function; factor analysis

J Nucl Med 2006; 47:330–336

Rodents have been widely used in biomedical research because of their relatively low cost and fast reproductive rate and because of the increasing availability of transgenic mice. Rodent models of human disease generally have lower experimental costs and take less time than studies with larger animals, such as dogs or baboons. With the introduction of high-resolution small-animal PET (e.g., microPET [Concorde Microsystems Inc.]) a decade ago (*1–3*), in vivo molecular imaging of small laboratory animals has become possible. With carefully designed radiotracers, high-resolution animal PET provides an effective and quantitative way to study human disease models, the pharmacokinetics of new drugs, molecular and cellular trafficking, gene expression, and protein–protein interactions. The growing interest in molecular imaging has led to the adoption of small-animal PET technology by more than 40 research institutions worldwide for the development of novel diagnostic and therapeutic agents (*4–7*).

Investigating changes in organ function, including myocardial function (e.g., blood flow, glucose metabolism, and free fatty acid metabolism), with the appropriate kinetic models requires accurate measurement of the blood input function and myocardial time–activity curve. Even with current detector technology, which provides improved spatial resolution, cardiovascular research with small-animal PET still is limited by the inherent spatial resolution of the system (partial-volume effects and spillover), as well as the rapid movement of the beating heart. The size of the rodent heart is small compared with the resolution of the system, making it difficult to extract artifact-free blood-pool input functions and myocardial time–activity curves from region of interests (ROIs) drawn on dynamic small-animal PET images.

A number of methods for measuring tracer activity concentrations in blood have been examined for application in kinetic models. Micro–blood sampling techniques are used routinely by our group (*8*). These techniques provide accurate blood input function measurements, but when multiple tracer studies are performed in the same animal, this technique is limited by the number of blood samples that can be withdrawn. Another method is the use of a β-probe, which lies inside (*9*) or alongside (*10,11*) a blood vessel. The placement of an arterial–venous shunt also was attempted but was complicated by both the counts originating from the tissue (*12*) and the complex microsurgical procedure. A noninvasive approach with a theoretic basis (predefined shape for the blood input function) and computer simulation for extracting the blood input function from mice imaged with a small-animal PET scanner has been described (*13*). This method was validated with ^{18}F-FDG kinetics in normal mice, and the theoretic basis of this method is applicable only to a limited number of animal

Received Mar. 31, 2005; revision accepted Nov. 15, 2005.

For correspondence or reprints contact: Michael J. Welch, PhD, Mallinckrodt Institute of Radiology, Washington University School of Medicine, Campus Box 8225, 510 S. Kingshighway Blvd., St. Louis, MO 63110.

E-mail: welchm@wustl.edu

models. The conventional noninvasive method currently used in a clinical PET setting requires the drawing of ROIs. However, when applied to dynamic small-animal PET images, this method is limited by large partial-volume effects and spillover from the rodent myocardium. This deficiency can be overcome by the use of factor analysis (FA) for the noninvasive extraction of the myocardial time–activity curve and the blood input function.

In the 1980s, FA was introduced in nuclear medicine (*14–18*). FA describes the covariance relationships among multiple variables in terms of a few underlying, but unobservable, random quantities called factors. All variables within a particular group are highly correlated. Variables in different groups have relatively small correlations. This method has been used to decompose dynamic images into component images and to determine their time–activity curves by analysis of the variance in the data (*14,15*). It has been reported that the FA method successfully extracts the input functions and myocardial time–activity curves from dynamic PET images of canines (*16,17*), humans (*16*), monkeys (*18*), and rats (*19*). In the rat study (*19*), the blood input functions were extracted with the FA method and were compared with those obtained from dynamic images by the ROI method. In the present study, the FA method was applied to dynamic small-animal PET images of rats and mice, and the time–activity curves generated were compared with those obtained from traditional blood samples.

MATERIALS AND METHODS

microPET R4

The microPET R4 was the first commercial PET scanner for rodents. Its design is based on the UCLA prototype (*1*) with improved sensitivity (*20*). The reconstructed-image resolution of the microPET R4 is 2.3 mm in full width at half maximum close to the center of the field of view. The volumetric resolution is ~5 μL at the center of the field of view on the basis of the 10-ns timing window and is less than ~14 μL within a 1-cm radius. A complete performance evaluation of the scanner was done by Knoess et al. (*20*).

Animal Studies

To investigate the accuracy of the FA method in determining the blood input function and myocardial time–activity curve, 2 groups of rodents were studied. The rodents had free access to standard rat chow and water. In group 1, 6 Sprague–Dawley rats (weight [mean ± SD], 305 ± 91 g) were studied with ^{18}F-FDG (n = 3) and 1-^{11}C-acetate (n = 3). In group 2, 6 BALB/c mice (weight, 20.8 ± 1.4 g) were studied with ^{18}F-FDG (n = 3) and 1-^{11}C-acetate (n = 3). The radiotracers (^{18}F-FDG and 1-^{11}C-acetate) were produced in our laboratory with a commercially available module (CTI Molecular Imaging).

Animal Preparations and Small-Animal PET Imaging

The use of animals was approved by the Animal Studies Committee at Washington University School of Medicine. Approximately 30 min before undergoing PET, rodents were anesthetized with inhalant anesthesia (1.5% isoflurane). Catheters were placed in the jugular vein for radiotracer administration and in the carotid artery for blood withdrawal during the scan. Rodents were placed in a supine position in the small-animal PET scanner.

All dynamic small-animal PET images were obtained with a microPET R4 housed in a temperature-controlled suite. After an intravenous bolus injection (100−150 μL) of ^{18}F-FDG (26.8 ± 4.5 MBq for rats and 24.1 ± 3.8 MBq for mice), list mode data were acquired for 60 min. The dynamic small-animal PET image data were sorted into 3-dimensional (3D) sinograms as follows: 24 frames of 5 s and 58 frames of 60 s. The frame durations were chosen to allow small intervals at early time points to show the rapid changes in the blood-pool input function and sampling at larger intervals at later time points to show the uptake characteristics of the myocardium. After an intravenous bolus injection of 1-^{11}C-acetate (32.7 ± 4.8 MBq for rats and 20.5 ± 5.5 MBq for mice) and because of the rapid kinetics of the tracer in the heart, list mode data were acquired for 20 min. Dynamic sorting of the data into 3D sinograms was performed as follows: 24 frames of 5 s, 12 frames of 15 s, 10 frames of 30 s, and 10 frames of 60 s. The frame durations were chosen on the basis of the dynamic imaging protocols used for 1-^{11}C-acetate in humans and large mammals studied at our institute.

The images were reconstructed by Fourier rebinning of the 3D sinograms followed by 2-dimensional filtered backprojection with a ramp filter (cutoff at Nyquist frequency). To obtain sufficient pixel density for analysis, the original images were enlarged with zoom factors of 3 and 4.225 for the rat and mouse studies, respectively, resulting in pixel sizes of 0.28 × 0.28 mm for the rat studies and 0.20 × 0.20 mm for the mouse studies. The slice thickness was 1.2 mm. At the time of the study, the only attenuation correction method available for this system was based on a ^{68}Ge point source and led to excessive noise in the transmission scans. Therefore, attenuation and scatter corrections were not applied. In general, attenuation correction factors are constant over time and should not change the shape of the time–activity curves. The time–activity curves were adjusted for their dynamic range on the basis of the maximum and minimum of the dynamic images and rescaled at the end of the FA procedure, as will be described in the next section. These steps effectively accounted for the scale introduced by attenuation and partially compensated for the bias introduced by scatter. Although the system is now equipped with appropriate attenuation and scatter corrections and the images it provides are more quantitative, we do not believe the absence of attenuation and scatter corrections significantly changed the results of the present study.

To compare blood-pool input functions obtained with the FA method to blood activity concentrations measured directly, arterial blood samples (mean ± SD volumes of blood were 6.1 ± 0.4 μL for rats and 5.9 ± 0.3 μL for mice) were withdrawn from the carotid artery catheter into Wiretrol II precision micropipette tubes (Drummond Scientific Co.). The dead volume of the catheter and sampling line was 50–100 μL, depending on the length of the catheter line and the size of the rodents used. During blood sampling, the catheter was not flushed, but a void sample was taken to ensure true blood sampling at each time point. For both types of animals and both radiotracers, blood samples were rapidly drawn for the scan duration (*8–10*). The micropipette tubes were preweighed and postweighed, and counting was done with a Beckman 3000 γ-counter for true blood activity concentration determinations.

FA Algorithm

FA assumes that the measured images are constructed from the superposition of a limited number of structures (or factors). For the present application, these structures correspond to the right ventricle, left ventricle, and myocardium. Each structure has a different time–activity curve, which is dependent on the kinetics of the tracer used. In the present study, we used the methodology of Di Paola et al. (*15*), which was extended by several groups (*16–19*). The FA method creates physiologic time–activity curves and their corresponding images in 4 steps. The flow chart in Figure 1 shows the processing steps used for FA.

First, 3 or 4 transaxial slices encompassing the heart were manually selected, and the data were added together. To remove or minimize the noise, data outside the specified organ area were masked from the images. The sizes of the masked transaxial images were 32×32 pixels for the mice and 40×40 pixels for the rats. The numbers of pixels as a function of time (time-dependent pixels) thus were 1,024 (32×32 pixels) for the mice and 1,600 (40×40 pixels) for the rats. Each time-dependent pixel in the masked images was normalized to the individual maximum value for each time-dependent pixel.

Second, after image processing, a principal components analysis was performed. The covariance matrix, eigenvectors, and eigenvalues (loadings) of the normalized time-dependent pixels were calculated for the 3 structures.

The third step was the determination of new factor axes that corresponded to the best representation without negative components for the 3 structures describing the dynamic data. These axes were calculated from the set of loading values for which the triangle subtended by the combination of any 3 loading values within the loading value space led to the maximum area. Thus, triangles were formed by any 3 loading values chosen out of 1,024 loading values for the mouse studies or 1,600 loading values for the rat studies. The normalized time–activity curves and the corresponding factor images were generated with these new factor axes. The final time–activity curves then were normalized by linear interpolation of the maximum and minimum values in the original images.

Finally, a constant given by the difference between the last data point for the FA blood input function and the last blood sample was added to left ventricle and right ventricle time–activity curves.

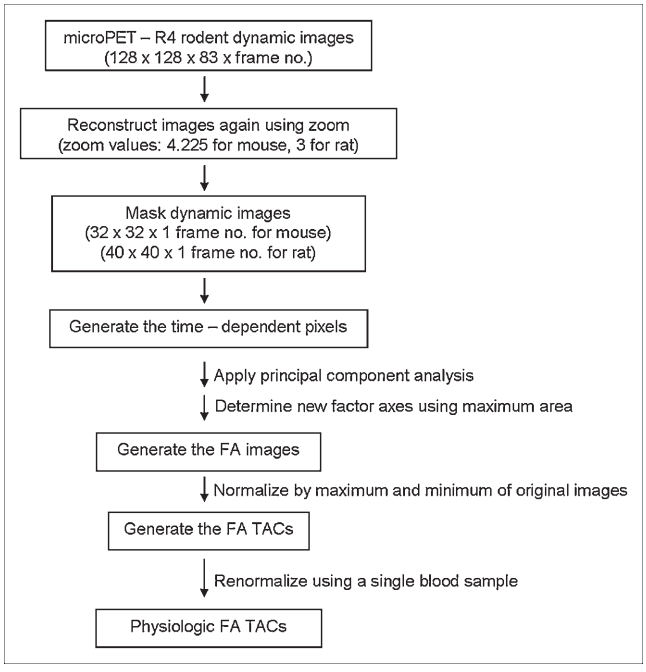

FIGURE 1. Flow chart of FA procedure used in this study. TACs = time–activity curves.

Statistical Analysis

Correlations and percentage errors for input functions extracted from blood samples and the FA method were calculated with linear least squares regression analysis.

RESULTS

The successful extraction of the factor images (right ventricle, left ventricle, and myocardium) of the heart of a living rat is shown in Figure 2B for the ^{18}F-FDG study and in Figure 2D for the 1-^{11}C-acetate study. The input functions obtained from the FA method and from the blood samples are shown in Figure 3 for the rats and in Figure 4 for the mice. In the ^{18}F-FDG rat studies, the slope of the regression line, the *y*-intercept, and the correlation coefficient for these 2 input functions were 1.13, −0.037, and 0.973, respectively (Fig. 5A). In the 1-^{11}C-acetate rat studies, the slope of the regression line, the *y*-intercept, and the correlation coefficient for these 2 input functions were 1.35, −0.054, and 0.965, respectively (Fig. 5B). The slope of the regression line, the *y*-intercept, and the correlation coefficients for the 2 input functions were 1.47, −0.480, and 0.930 in the ^{18}F-FDG mouse studies (Fig. 5C) and 1.17, 0.062, and 0.972 in the 1-^{11}C-acetate mouse studies (Fig. 5D), respectively. Linear regression data and percentage errors for the 2 input functions were obtained from the blood samples and the FA method. The correlation coefficient of all studies averaged 0.96 ± 0.02, whereas the slope was consistently larger than 1 (by an average of ~28%). Correlation functions with a slope of 1 are represented by dashed lines on Figure 5 for comparison.

DISCUSSION

The FA method was able to adequately extract the blood input function in PET studies of rats and mice. The next generation of scanners (*21*), with improved spatial resolution or the use of advanced image reconstruction algorithms incorporating resolution recovery for the loss of resolution because of the system response (*22,23*), may eventually improve the extraction of artifact-free blood time–activity curves from images.

For several decades, rodent blood sampling techniques have been used with a variety of tracers to quantify glucose metabolism and blood flow (*24–26*) in rats and in mice (*27,28*). A comparison of glucose metabolic rates in rats and humans demonstrated a good correlation (*28*), showing that rapid arterial blood sampling in rodents produces an accurate input function. Huang et al. (*13*) described a theoretic approach to blood flow measurements, combined with limited blood sampling, in individual animals over a large population. This statistical analysis–based method

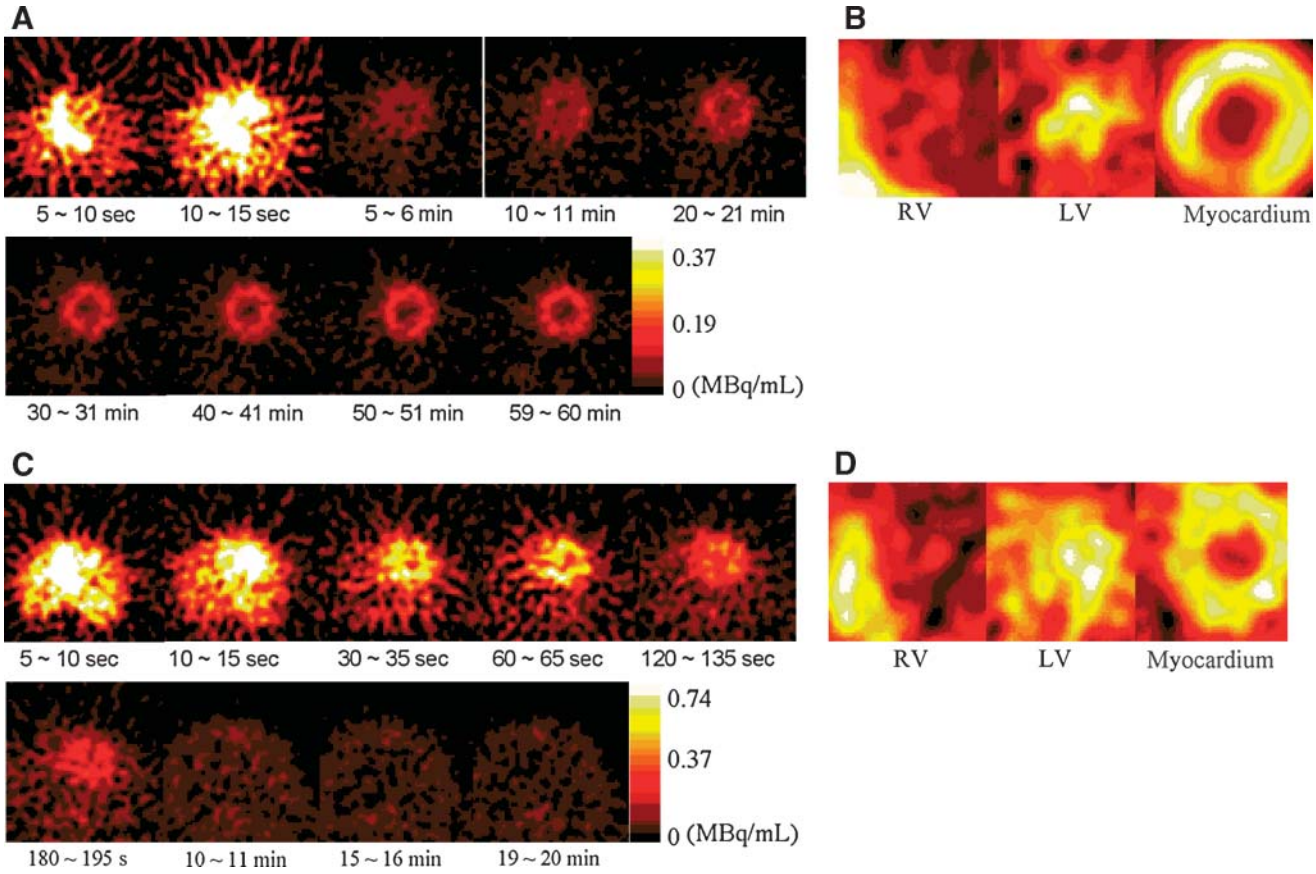

FIGURE 2. (A) Representative ^{18}F-FDG dynamic images (transaxial slices) of rat (weight: 279 g; injection dose: 29.9 MBq). (B) Representative factor images of right ventricle (RV), left ventricle (LV), and myocardium obtained from A. (C) Representative 1-^{11}C-acetate dynamic images (transaxial slices) of rat (259 g; 38.3 MBq). (D) Factor images of RV, LV, and myocardium obtained from C.

discriminated inaccurate input functions from real input functions on the basis of a comparison of simulated blood sampling and image-derived input functions, each with its own associated errors. Bentourkia et al. (*19*) showed that the blood input function in rats could be extracted from the left ventricle with FA, but this method was not validated against blood sampling.

In the rat studies in this report, we could extract the 3 factor images (right ventricle, left ventricle, and myocardium) and generate time–activity curves for each factor image using the FA method. The FA input function agreed well with that obtained from blood sampling in the ^{18}F-FDG and 1-^{11}C-acetate rat studies. This finding shows that although PET images of rats are subject to partial-volume effects and cardiac motion blurring, the FA method overcomes these potential limitations and is able to produce a true blood input function from either right ventricle or left ventricle factors.

The FA input function (extracted from the right ventricle factor) agreed well with that obtained from direct blood sampling in the ^{18}F-FDG and 1-^{11}C-acetate mouse studies. However, the left ventricle time–activity curve had a shape similar to the summation of the right ventricle blood input function and myocardial time–activity curve, indicating that the left ventricle time–activity curve was contaminated by the myocardial time–activity curve. As a result, the factor image of the left ventricle showed contributions from the factor images of both the blood pool and the myocardium. Because of the very small size of the mouse heart compared with the resolution of the system, it was extremely difficult to distinguish suborgan structures and to extract their time–activity curves from dynamic PET images with any image-based methods, including FA. The application of FA in mice therefore showed limitations when an imaging system with insufficient resolution was used. It is possible that the next generation of scanners will allow for more accurate FA in mice.

As mentioned in the Results section, the slope of the linear regression lines was consistently greater than unity. In general, the image-derived time–activity curves yielded higher peak maxima than the well counter blood sample data, suggesting an underestimation of the peaks even when rapid blood sampling techniques were used and leading to the slopes observed in Figure 5. Similar observations were made by Wu et al. (*18*), who compared the input function derived from an ROI in the left ventricle of small primates with the input function derived from blood sampling and well counting.

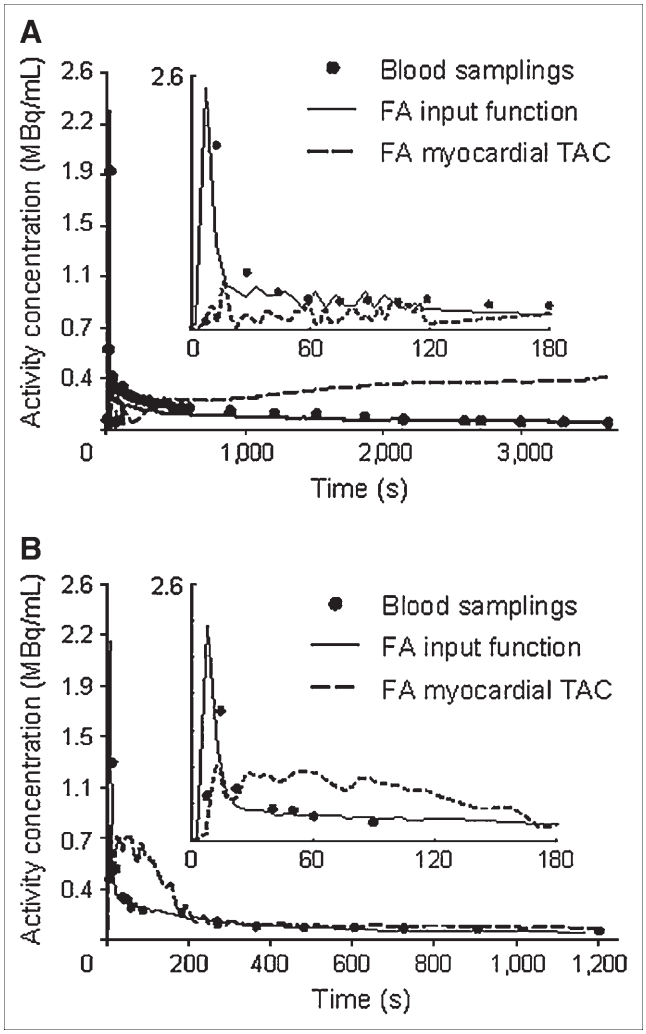

FIGURE 3. Time–activity curves (TAC) obtained with blood sampling and FA method in rat studies. Insets show first 3 min of time–activity curves. (A) Blood-pool input functions generated by blood sampling and FA method in ^{18}F-FDG rat study ($r = 0.96 \pm 0.01$, $n = 3$). (B) Blood-pool input functions obtained by blood sampling and FA method in 1-^{11}C-acetate rat study ($r = 0.97 \pm 0.02$, $n = 3$).

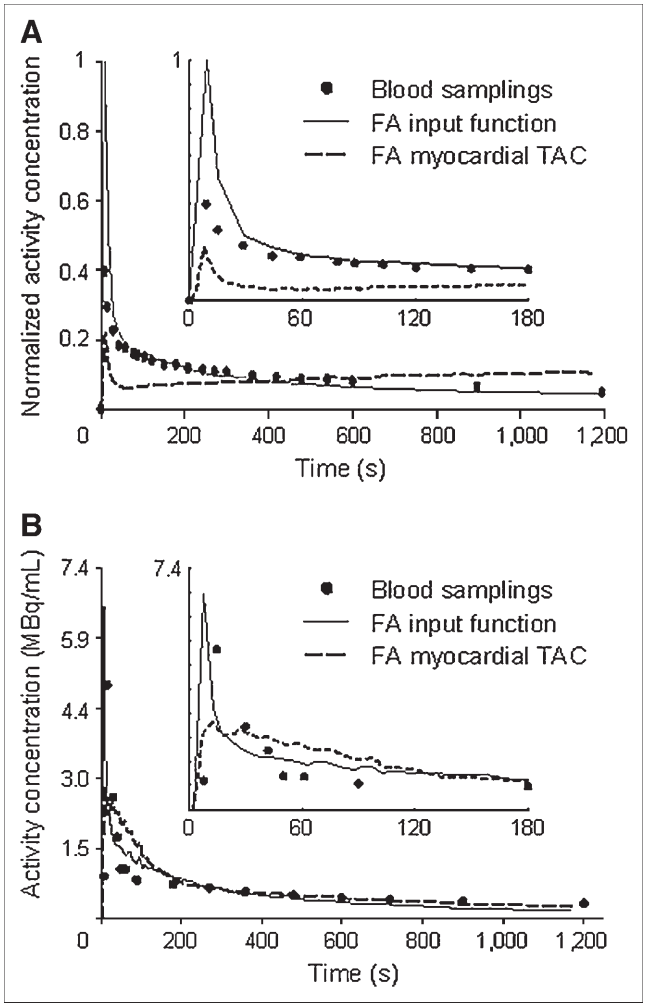

FIGURE 4. Time–activity curves (TAC) obtained with blood sampling and FA method in mouse studies. Insets show first 3 min of time–activity curves. (A) Input function and myocardial time–activity curve in mouse study with ^{18}F-FDG. FA input function was rescaled with blood sample obtained at 20 min after administration. (B) Input function and myocardial time–activity curve in mouse study with 1-^{11}C-acetate. It was not possible to extract myocardial time–activity curve by ROI method because of partial-volume effects and spillover.

As anticipated, the shapes of FA myocardial time–activity curves obtained from mouse and rat studies were similar. Residual spillover from the blood pool still existed and could be seen as a peak at early time points on the FA time–activity curves. There is no current standard for extracting myocardial time–activity curves from rodent data for comparison with myocardial time–activity curves generated from FA. In both radiotracer studies, myocardial time–activity curves were not corrected for residual partial-volume effects and spillover, and the FA blood-pool input function was not corrected for metabolite activity. Therefore, the measured ratio of myocardium to blood-pool activity concentrations appeared to be smaller than the expected value. Nevertheless, for extracting the blood input function from dynamic images, the FA method has an obvious advantage over the ROI method. FA allows a clear separation of the different compartments for an imaging system characterized by a given spatial resolution. FA and image-based extraction of blood input functions and myocardial time–activity curves of rodents may be improved by the use of cardiac gated dynamic images (*29*) or a higher-resolution small-animal PET scanner (*21*).

Such advances may further improve the performance of the FA method and lead to the replacement of multiple blood sampling in rodent studies.

CONCLUSION

The present study has demonstrated that the FA method can minimally invasively obtain input functions and myocardial time–activity curves from dynamic small-animal PET images of rodents, a goal that was not possible with

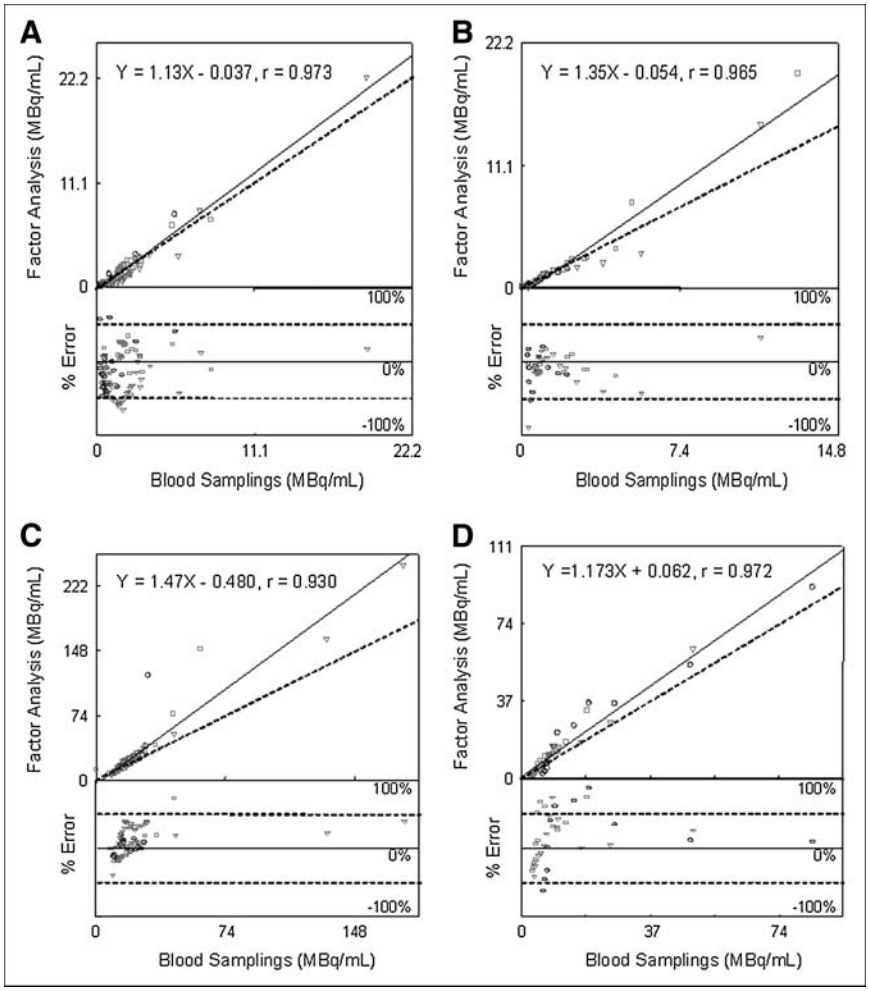

FIGURE 5. Linear regression line (—) and percentage error plot for input functions obtained from blood sampling and FA method. Percentage error was calculated from difference between FA values and blood sample values. Dashed line is unity line ($y = x$). (A) ^{18}F-FDG rat studies ($n = 3$). (B) 1-^{11}C-Acetate rat studies ($n = 3$). (C) ^{18}F-FDG mouse studies ($n = 3$). (D) 1-^{11}C-Acetate mouse studies ($n = 3$).

ROI-based methods. Therefore, the FA method enables reliable quantification of physiologic or biologic information generated in small-animal PET studies and does not require the drawing of ROIs on small structures, such as a rodent heart or other small organs of interest, or repeated blood sampling.

This technique has been used to quantify myocardial blood flow in rats (*30*), in which the measurement has been validated by comparison with the gold standard radioactive microsphere method. In addition, it has been used to quantify myocardial metabolism in the Zucker rat model of diabetes (*31*). In these 2 instances, this technique has been used to quantify important cardiac metabolic parameters.

ACKNOWLEDGMENTS

We thank Nicole Fettig, Lori Strong, Margaret Morris, Mark Nolte, Jerrel Rutlin, and Lynne Jones for technical assistance. We thank Kooresh Shoghi for helpful discussions and Joanna Downer for help in proofreading the manuscript. This work was supported by NIH/NHLBI grant 2-PO1-HL-13851.

REFERENCES

1. Cherry SR, Shao Y, Silverman RW, et al. microPET: a high resolution PET scanner for imaging small animals. *IEEE Trans Nucl Sci.* 1997;44:1161–1166.
2. Chatziioannou AF, Cherry SR, Shao Y, et al. Performance evaluation of microPET: a high-resolution lutetium oxyorthosilicate PET scanner for animal imaging. *J Nucl Med.* 1999;40:1164–1175.
3. Lecomte R, Cadorette J, Richard P, et al. Design and engineering aspects of a high resolution positron tomograph for small animal imaging. *IEEE Trans Nucl Sci.* 1994;41:1446–1452.
4. Hove JD, Iida H, Kofoed KF, et al. Left atrial versus left ventricular input function for quantification of the myocardial blood flow with nitrogen-13 ammonia and positron emission tomography. *Eur J Nucl Med Mol Imaging.* 2004;31:71–76.
5. Inubushi M, Jordan MC, Roos KP, et al. Nitrogen-13 ammonia cardiac positron emission tomography in mice: effects of clonidine-induced changes in cardiac work on myocardial perfusion. *Eur J Nucl Med Mol Imaging.* 2004;31:110–116.
6. Inubushi M, Wu JC, Gambhir SS, et al. Positron-emission tomography reporter gene expression imaging in rat myocardium. *Circulation.* 2003;107:326–332.
7. Kudo T, Fukuchi K, Annala AJ, et al. Noninvasive measurement of myocardial activity concentrations and perfusion defect sizes in rats with a new small-animal positron emission tomograph. *Circulation.* 2002;106:118–123.
8. Sharp TL, Dence CS, Engelbach JA, et al. Techniques necessary for multi-tracer quantitative small-animal imaging studies. *Nucl Med Biol.* 2005;32:875–884.
9. Pain F, Laniece P, Mastrippolito R, et al. Arterial input function measurement without blood sampling using a β-microprobe in rats. *J Nucl Med.* 2004;45:1577–1582.
10. Kudomi N, Choi E, Yamamoto S, et al. Development of a GSO detector assembly for a continuous blood sampling system. *IEEE Trans Nucl Sci.* 2003;50:70–73.

11. Yamamoto S, Tarutani K, Suga M, et al. Development of a phoswich detector for a continuous blood-sampling system. *IEEE Trans Nucl Sci.* 2001;48: 1408–1411.
12. Votaw J, Shulman SD. Performance evaluation of the pico-count flow-through detector for use in cerebral blood flow PET studies. *J Nucl Med.* 1998;39: 509–515.
13. Huang SC, Wu HM, Shoghi-Jadid K, et al. Investigation of a new input function validation approach for dynamic mouse microPET studies. *Mol Imaging Biol.* 2004;6:34–46.
14. Barber DC. The use of principal components in the quantitative analysis of gamma camera dynamic studies. *Phys Med Biol.* 1980;25:283–292.
15. Di Paola R, Bazin JP, Aubry F, et al. Handling of dynamic sequences in nuclear medicine. *IEEE Trans Nucl Sci.* 1982;NS29:1310–1321.
16. Wu HM, Hoh CK, Choi Y, et al. Factor analysis for extraction of blood time–activity curves in dynamic FDG-PET studies. *J Nucl Med.* 1995;36: 1714–1722.
17. Wu HM, Hoh CK, Buxton DB, et al. Quantification of myocardial blood flow using dynamic nitrogen-13-ammonia PET studies and factor analysis of dynamic structures. *J Nucl Med.* 1995;36:2087–2093.
18. Wu HM, Huang SC, Allada V, et al. Derivation of input function from FDG-PET studies in small hearts. *J Nucl Med.* 1996;37:1717–1722.
19. Bentourkia M, Lapointe D, Selivanov V, Buvat I, Lecomte R. Determination of blood curve and tissue uptake from left ventricle using FADS in rat FDG-PET studies. Paper presented at: 1999 IEEE Nuclear Science Symposium and Medical Imaging Conference; October 24–30, 1999; Seattle, WA.
20. Knoess C, Siegel S, Smith A, et al. Performance evaluation of the microPET R4 PET scanner for rodents. *Eur J Nucl Med Mol Imaging.* 2003;30: 737–747.
21. Tai YC, Chatziioannou AF, Yang Y, et al. microPET II: design, development and initial performance of an improved microPET scanner for small-animal imaging. *Phys Med Biol.* 2003;48:1519–1537.
22. Qi J, Leahy RM. Resolution and noise properties of MAP reconstruction for fully 3-D PET. *IEEE Trans Med Imaging.* 2000;19:493–506.
23. Qi J, Leahy RM, Cherry SR, et al. High-resolution 3D Bayesian image reconstruction using the microPET small-animal scanner. *Phys Med Biol.* 1998;43: 1001–1013.
24. Sakurada O, Kennedy C, Jehle J, et al. Measurement of local cerebral blood flow with iodo [^{14}C] antipyrine. *Am J Physiol.* 1978;234:H59–H66.
25. Savaki HE, Davidson L, Smith C, et al. Measurement of free glucose turnover in brain. *J Neurochem.* 1980;35:495–502.
26. Bontempi B, Beracochea D, Jaffard R, et al. Reduction of regional brain glucose metabolism following different durations of chronic ethanol consumption in mice: a selective effect on diencephalic structures. *Neuroscience.* 1996;72:1141–1153.
27. Sokoloff L, Reivich M, Kennedy C, et al. The [^{14}C]deoxy-glucose method for the measurement of local cerebral glucose utilization: theory, procedure, and normal values in the conscious and anesthetized albino rat. *J Neurochem.* 1977;28:897–916.
28. Blin J, Ray CA, Chase TN, Piercey MF. Regional cerebral glucose metabolism compared in rodents and humans. *Brain Res.* 1991;568:215–222.
29. Rowland DJ, Newport DF, Laforest R, et al. Respiratory and cardiac gating on the microPET scanner [abstract]. *Molecular Imaging Biol.* 2003;5:124.
30. Herrero P, Kim J, Sharp TL, et al. Assessment of myocardial blood flow using ^{15}O-water and 1-^{11}C-acetate in rats with small-animal PET. *J Nucl Med.* In press.
31. Welch MJ, Lewis JS, Kim J, et al. Assessment of myocardial metabolism in diabetic rats using small-animal PET imaging: a feasibility study. *J Nucl Med.* In press.